BNL-212462-2019-TECH
C-A/AP/628

Effective ZDC cross section measurement during a dedicated STAR elastic scattering physics store in Run15

A. Drees

November 2019

Collider Accelerator Department
Brookhaven National Laboratory

U.S. Department of Energy
USDOE Office of Science (SC), Nuclear Physics (NP) (SC-26)

DISCLAIMER

Effective ZDC cross section measurement during a dedicated STAR elastic scattering physics store in Run15

A. Drees

November 7, 2019

1 Introduction

At RHIC the collision rate per IP is monitored by the Zero Degree Calorimeters (ZDC) [1] during most runs. Neutral particles produced in the collisions in the forward direction are detected in the ZDC and the collision rate corresponds to the rate of mutual neutrons above a variable threshold and within a certain coincidence window. Due to potential changes in the detector setup, configuration and electronics the ZDCs are calibrated every year by the use of vernier scans [2].

At the end of the RHIC pp run in 2015 a dedicated run for the STAR elastic scattering physics program (PP2PP) was scheduled during which a total of 3 vernier scans was performed within the same store. This note presents the data and summarizes the results, i.e. effective ZDC cross section and the associated systematic errors from those scans.

2 PP2PP 2015 Vernier Scans

All three vernier scans listed in Tab. 1 were done during the same store (18915) on Apr. 16 2015. The ramp file used to bring the two beams into collisions was "pp15-rot_1429180959" with design beta functions of $\beta^*_H = 0.87$ m and $\beta^*_V = 0.83$ m and a beam energy of 100 GeV. During the scans the transverse size and shape of the beam overlap

fill	beam moved	time	intensity
18915_1	Y	11:26 - 11:43	209 10^{11} x 203 10^{11}
18915_2	B	14:06 - 14:23	200 10^{11} x 200 10^{11}
18915_3	Y	15:20 - 15:38	197 10^{11} x 199 10^{11}

Table 1: List of vernier scans during the 2015 PP2PP run. The fill pattern was 111x111 bunches with 102 colliding pairs in IP6.

region was measured by recording the interaction rate as a function of the transverse beam separation. The maximum beam separation of $\pm$ 900μm was reached in a series of 6 steps of 150μm each. A fit of the collision rates as a function of the separation, in this case the measured ZDC coincidence rate, allows to determine the effective beam size, and thus

the emittance, as well as the maximum achievable coincidence rate and the effective cross section of the detector in use (ZDC). Typically, additional effects such as possible crossing angles, the difference between the set separation and the measured separation, the amount of debunched beam (if any) or the hourglass effect might require correction factors and/or systematic errors to be applied.

2.1 The Fit Function

The shape of the overlap region, i.e. the collision rate $R_{coll}(x)$ as a function of distance between the two beams, x, is mapped by the vernier scan and can usually be described by a single Gauss-function:

$$R_{\rm coll}(x) \;=\; R_{\rm Bkgd} \;+\; R_{\rm max} \;\times\; \exp\left(\frac{-(x-x_0)^2}{2\,\sigma_{\rm x}^{\rm VS}}\right) \tag{1}$$

with the following 4 free parameters:
$R_{\rm Bkgd}$: non-collision related background signal in the collision rate
$R_{\rm max}$: maximum collision rate seen by the ZDC detector (corrected for background)
x_0: location of the maximum
σ_x: width of the overlap region
The application and DAQ software that supports fully automated vernier scans at STAR employs single-Gauss fits for its online analysis [3].

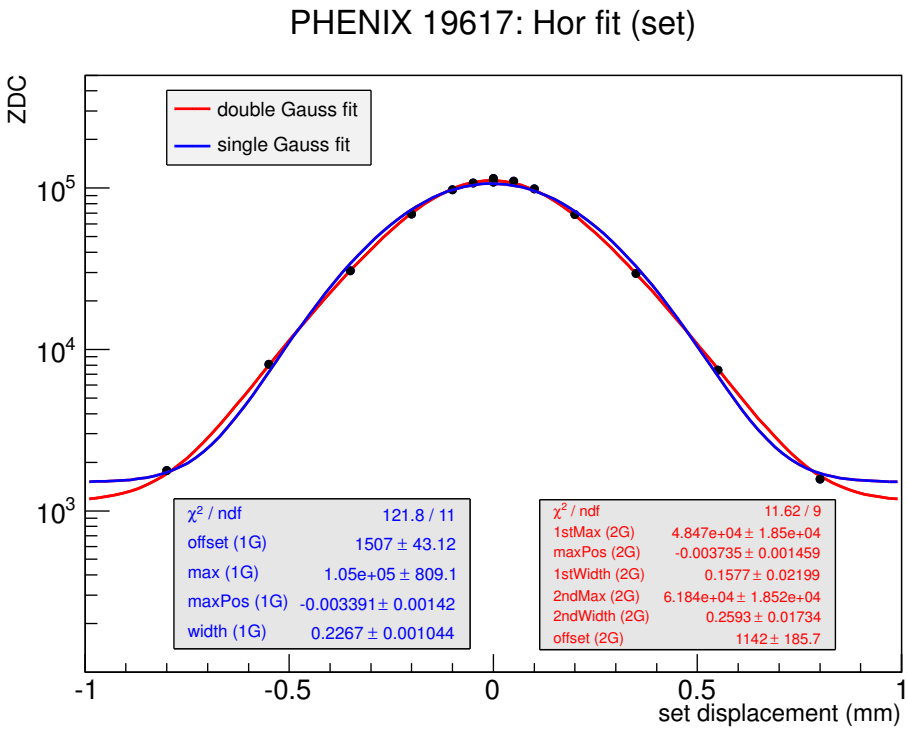

Figure 1: The signal from the PHENIX experiment ZDCs fitted with a 1-Gauss and a 2-Gauss fit function. The 2-Gauss fit function in this case is favored by about a factor 10 in χ^2/ndf. This fill was selected for demonstration purpose only.

Sometimes, as in the case of proton beams at 255 GeV for example, the single Gauss approach does not necessarily fit the data best, as shown in Fig. 1. If that's the case, a double Gauss-function is chosen:

$$R_{\mathrm{coll}}(x) \;=\; R_{\mathrm{max,1}} \;\times\; \exp\left(\frac{-(x-x_0)^2}{2\,\sigma_{\mathrm{x,1}}^{\mathrm{VS}}}\right) \;+\; R_{\mathrm{max,2}} \;\times\; \exp\left(\frac{-(x-x_0)^2}{2\,\sigma_{\mathrm{x,2}}^{\mathrm{VS}}}\right) \qquad (2)$$

The double Gauss function has 5 free parameters:
$R_{\mathrm{max,1}}$: maximum collision rate of the core region
x_0: location of both the maxima
$\sigma_{\mathrm{x,1}}$: width of the core overlap region
$R_{\mathrm{max,2}}$: maximum of the tail distribution
$\sigma_{\mathrm{x,2}}$: width of the tail region

The double Gauss approach is typically not needed to describe the data for protons at 100 GeV or lower intensity Heavy Ions. Its necessity was first observed during Run-9 [4]. However, the double Gauss approach gives more consistent results even if applied for 100 GeV proton beam energies as shown in Tab. 2. If chosen, it is assumed that both Gauss distributions, core and tail, are centered around the same location x_0. For the PP2PP run in 2015 the χ^2/ndf for the single Gauss fit is by far not as large as in Figure 1 and in the single digit range (see Tab. 2). While the double Gauss fit was used as the default option, both fitting approaches were used to compute the final value and a systematic error is assigned to this uncertainty in our knowledge of the beam shape. The cross sections listed in Tab. 2 are mostly uncorrected, except for a correction for accidental coincidences (section 4.2) since this correction is applied to the raw 1 Hz-signal on a point-by-point basis. See Tab. 4 in section 5 for the fully corrected cross sections.

fill	1G [mbarn]	χ^2/ndf H/V	2G [mbarn]	χ^2/ndf H/V
18915_1	0.261	0.4 / 3.2	0.269	0.1 / 1.3
18915_2	0.256	0.7 / 0.9	0.268	0.7 / 0.9
18915_3	0.253	1.0 / 2.2	0.268	1.0 / 2.2

Table 2: Effective uncrorrected cross sections (except point-by-point corrections) and χ^2/ndf values per plane using the single Gauss (1G) and double Gauss (2G) approach.

3 The Effective Cross Section

The effective detector cross section $\sigma_{\mathrm{ZDC}}^{\mathrm{eff}}$ of a detector, in this case the ZDCs, can be determined by the beam current, the collision rate and the overlap region $\sigma_{\mathrm{x,y}}^{\mathrm{VS}}$ of the two beams. The maximum collision rate and the width of the overlap region are derived from the fits to the vernier scan data.

$$\sigma_{\mathrm{ZDC}}^{\mathrm{eff}} = \frac{R_{\mathrm{max}}\; 2\pi\; n_B\; n_Y\; \sigma_{\mathrm{x}}^{\mathrm{VS}}\; \sigma_{y}^{\mathrm{VS}}}{n_{\mathrm{coll}}\; f_{\mathrm{rev}}\; N_B\; N_Y} \qquad (3)$$

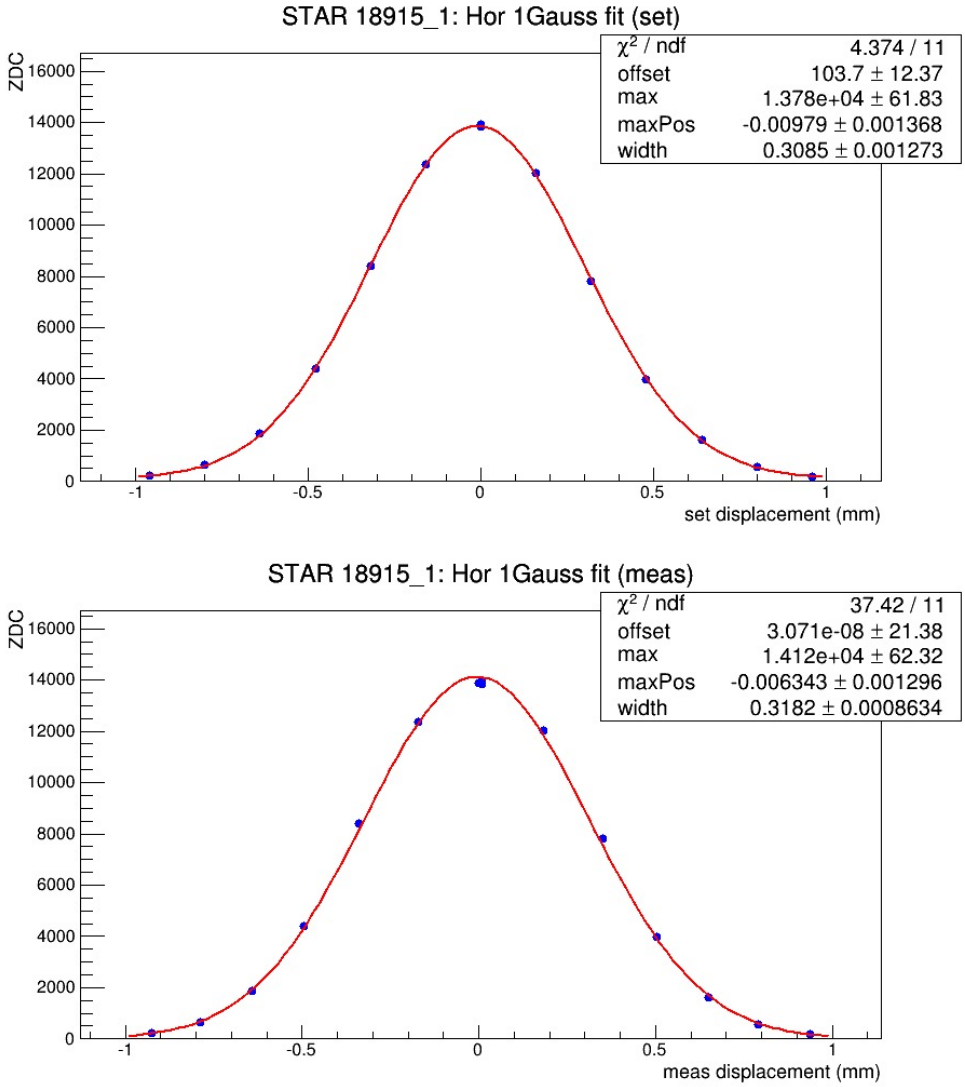

Figure 2: Data from a horizontal vernier scan at IP6, 18915_1. Each data point corresponds to a measurement interval of 30 sec. In this case a 1-Gauss fit was chosen. The top graph shows the ZDC rates as a function of the design separation, the bottom is the same data as a function of the separation measured by the BPMs.

where:
$R_{\rm max}$ = maximum collision rate seen by the ZDC detector (corrected for background)
n_B, n_Y = number of blue and yellow bunches respectively
$\sigma^{\rm VS}_{\rm x,y}$ = width of the beam-overlap area, derived from the fit to the vernier scan data
$n_{\rm coll}$ = number of colliding bunch pairs in the IP where the ZDC detector is located
$f_{\rm rev}$ = revolution frequency, approx. 78.4 kHz
$N_{\rm B,Y}$ = total number of blue and yellow protons, from DCCT

Figure 2 shows one example of a vernier scan, here in the horizontal plane, moving the yellow beam. The top graph depicts the ZDC coincidence rate as a function of the

set value, the bottom depicts the ZDC coincidence rate as a function of the measured distance between the two beams. Both are fitted with a single Gauss-function according to Equation 1. The χ^2/ndf in the top graph (using set values from the model) is significantly smaller than in the bottom graph (using measured distances), demonstrating that using the measured displacements (i.e. data from the DX BPMs) does not reproduce the data as well. This appears in all three PP2PP scans in 2015 and requires a more systematic study. The beam overlap size σ^{VS} in Equation 3 is given by the combination of the two widths from the double Gauss fit. Here, the combined width is obtained by adding the two individual widths normalized with their amplitudes [4]:

$$\sigma_{\mathrm{x,y}}^{\mathrm{comb}} = \sigma_1^{\mathrm{x,y}} \frac{R_{\mathrm{max},1}}{R_{\mathrm{max},1} + R_{\mathrm{max},2}} + \sigma_2^{\mathrm{x,y}} \frac{R_{\mathrm{max},2}}{R_{\mathrm{max},1} + R_{\mathrm{max},2}} \tag{4}$$

"x" and "y" refer to the two planes, while "1" and "2" refer to the core (1) and tail (2) part of the distribution respectively. Once the measured widths from the two approaches, using set or measured distances, are combined they typically agree to better than 5 μm.

Several corrections are applied to the cross section and/or emittance measurement using the vernier scan method. They affect the collision rate (accidental coincidences and for some detectors the hour-glass effect), the beam current measurement (fill pattern and debunched beam) and the measurement of the width (hour-glass, crossing angle, beam-beam, model inaccuracy). These effects are outlined below.

4 Corrections

4.1 Beam Current and Fill Pattern

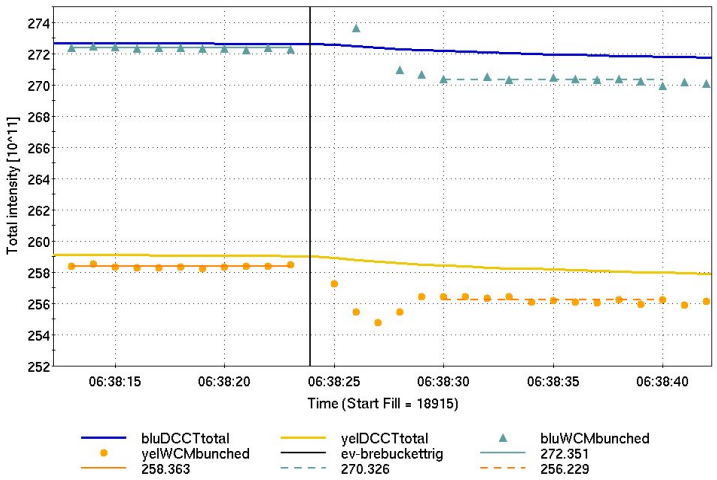

Figure 3: Beam current measured by DCCT and WCM during the rebucketing process at the beginning of store 18915.

The collision rate, i.e. the ZDC coincidence rate, is corrected for the continuous decrease of the beam current point-by-point. For this correction the total circulating beam is used as measured by the DCCTs [5]. **Beam current measurements by the DCCT carry a 0.2% additional systemtatic error**. During routine proton running without

a failure, no beam debunching is expected. Therefore, measurements from the WCM [5] (total bunched beam) can be ignored for the most part. This assumes that, with protons, all beam is bunched. While there is no ongoing debunching of proton beams during the store, beam could still debunch at the time of rebucketing or due to a RF failure (if any). There were no RF failures in store 18915 but there could have been a loss of bunched beam during rebucketing that is going unnoticed by the DCCTs. Bunched beam loss, which appears only in the WCM measurement, is difficult to measure since there is a habitual discrepancy between the WCM and the DCCT that changes when the WCM changes its gain setting (about 10 times per store) and the WCM measurement will change accordingly by up to $\pm$ 2% at times. Such automatic gain adjustments will also happen at the time of rebucketing. One cannot distinguish between a loss of bunched beam and the appearance of a change in beam current due to gain changes. Fig. 3 depicts the rebucketing phase at the beginning of store 18915. The blue and yellow solid lines represent the total beam current as measured by the DCCTs. The turquois and orange triangles and dots are the blue and yellow WCM measurement respectively. The black vertical line indicates the start time of the rebucketing. The large variations visible in the WCM measurement right after rebucketing are due to the aforementioned gain changes in the WCM read-out electronics. The solid turquois and orange lines are the averaged WCM reading before rebucketing while the turquois and orange dashed lines are the averaged WCM readings after rebucketing. The loss of bunched beam comes to 2.02 10^{11} protons in blue and 2.13 10^{11} protons in yellow, about a 1% loss per ring. While this beam is debunched and not contributing to collisions, it is still circulating in the machine and is detected by the DCCTs as part of the total circulating beam current. If the correction is applied to the beam current as measured by the DCCT, this loss changes the cross section by 2%, which can be corrected for. But, due to the uncertainties in the measurement (i.e. the gain changes in the scope), **we apply only half of the measured drop and add a 1% systematic error to the result**. This correction factor of 0.990 appears as $R_{debBeam}$ in the final equation for the corrected cross section, Eq. 12.

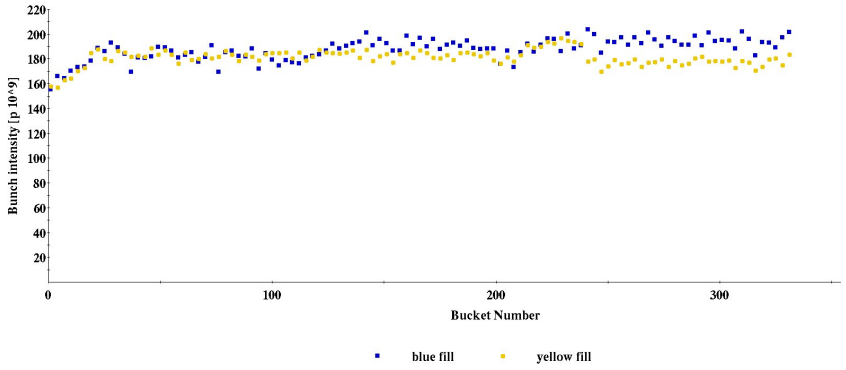

Figure 4: Bunch by bunch beam current measured by WCM during store 18915.

In Equation 3 the beam current in each bunch is given as the total number of protons per ring divided by the number of bunches in blue and yellow respectively: $N_{\mathrm{total}}/\mathrm{n_{B,Y}}$, thus using an average bunch intensity. This approach relies on a uniform distribution of the total beam over the bunches in the rings. Large bunch intensity fluctuations could potentially change the actual product depending on the actual colliding pairs of bunches

and their individual intensities. The colliding pairs are different at the two IPs. Figure 4 shows the fill pattern during store 18915 as the bunches are paired in IP8 and IP2. In IP6, or PP2PP, the bunch trains are shifted such that blue bunch number 41 lines up with yellow bunch number 1. The difference between the sum of the correct individual pairs and the sum of the averaged pairs is +0.48% and can be corrected for. Therefore, no additional systematic error is assigned. This correction facor of 1.005 appears as R_{FP} in the final equation for the fully corrected cross section, Eq. 12.

4.2 Accidental Coincidences

The collision rate, defined by the ZDC coincidences, is contaminated by false, or accidental, coincidence signals caused by high singles rates. Singles rates, i.e. the signal from just one side of the ZDC detector, contain a large amount from the coincidence signal and an even larger portion of unrelated signals that are typically from collisions but not from mutually forward neutral particles. The signal from the blue-incoming side is referred to as $\mathrm{ZDC_B}$, and from the yellow-incoming side as $\mathrm{ZDC_Y}$. A purely statistical approach to correct for accidental coincidences yields:

$$\mathrm{ZDC_{BY}} = \frac{\mathrm{ZDC_B\ ZDC_Y\ n_{coll}}}{\mathrm{n_B\ n_Y}\ f_{\mathrm{rev}}} \tag{5}$$

$$\mathrm{ZDC_{corr}} = \mathrm{ZDC_{raw}} - \mathrm{ZDC_{BY}} \tag{6}$$

with the parameters equivalent to Eq. 3 and $\mathrm{ZDC_{raw}}$ corresponding to the uncorrected collision rate. This approach overestimates the number of accidental coincidences by hits in the two sides of the ZDC detector that lead to coincidence hits but are not true beam crossing events. The following Equation corrects for multiple hits that are counted as a single hit and contains the correction for accidental hits from above [6]:

$$\mathrm{ZDC_{log.corr}} = \mathrm{n_{coll}}\ f_{\mathrm{rev}}\ \left(-ln\left(1 - \frac{\mathrm{ZDC_{raw}} - \mathrm{ZDC_{BY}}}{\mathrm{n_{coll}} f_{\mathrm{ref}} + \mathrm{ZDC_{raw}} - \mathrm{ZDC}_B - \mathrm{ZDC}_Y}\right)\right) \tag{7}$$

This correction is applied point-by-point to the raw signal and varies significantly as the store progresses. Figure 5 demonstrates the effect and amount of the two different corrections. The graph shows the uncorrected ZDC coincidence rates for STAR ("_RawCoinc"), the coincidence rates corrected according to Eq. 6 ("_StandardCorrected") and the coincidence rates corrected using Eq. 7 ("_LogCorrected"). The top graph presents the ratio of the LogCorrected rates to the StandardCorrected rates. The difference starts out at about 10% and drops to about 3% at the end of the store. This signifies the amount of over-correction when using a purely statistical approach according to Eq. 6. Once the corrections are applied to the ZDC coincidence signal, the ratio of PHENIX to STAR should be constant. Any variation from this constant ratio indicates a systematic uncertainty of the accidentals correction. Fig. 6 shows the variation of this ratio as a function of time for two signals from the two experiments. The red line represents the fully corrected luminosity signal ratio and the black line the ratio of the two raw ZDC coincidence signals. The average values of the two ratios are shown as a green dashed (fully corrected signal ratio) and yellow dashed line (raw signal ratio) respectively. The ratio shows a more systematic deviation from the average constant value at the beginning of the stores as well as an over-all, statistical, scatter. The deviation from a constant at the beginning of the store indicates an over- or under-correction when using Eq. 7. The distribution of the ratio

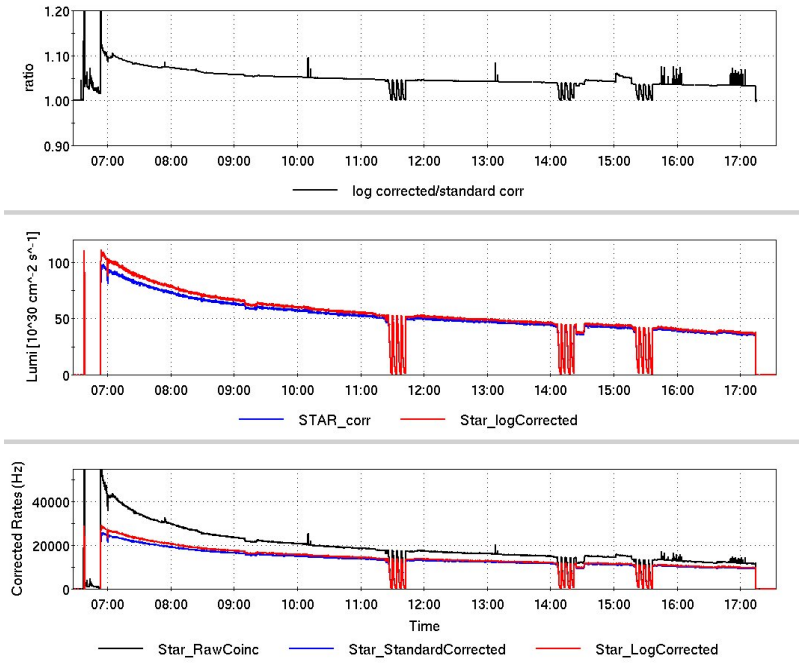

Figure 5: Bottom: ZDC uncorrected and corrected coincidence rates, center: standard corrected and log corrected luminosity, top: ratio of the two different corrections, all during store 18915.

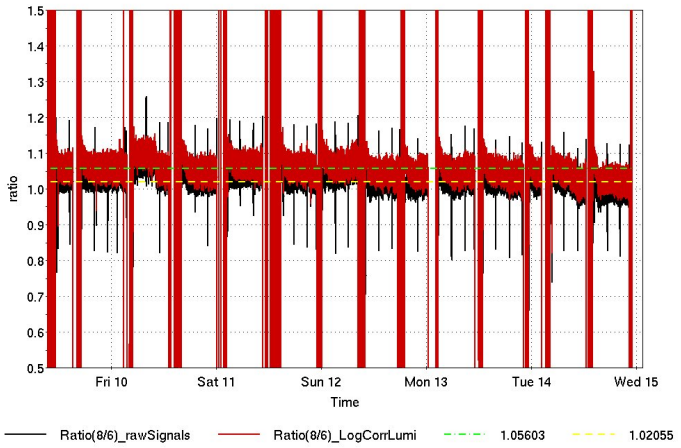

Figure 6: The ratio of the raw and fully corrected signals from the two experiments in 2015, STAR and PHENIX, as a function of time for the period of about one week prior to store 18915.

around its average value is shown on the left in Fig. 7. It has an RMS value of 2.4%. The actual mean value simply indicates that the PHENIX experiment saw a 5.6% higher collision rate in run 15 when compared to STAR. Due to the alignment of the two abort gaps in the PHENIX IP, this is to be expected. However, a large fraction of this scatter is of purely statistical nature and already included in the statistical error. The statistical fluctuations for one randomly picked store (18908) prior to the PP2PP store 18915 is shown in Fig. 7 on the right. It shows an RMS of 1.5%. **Therefore, a systematic store-to-store error of 1% is assigned to the accidental correction**. The correction

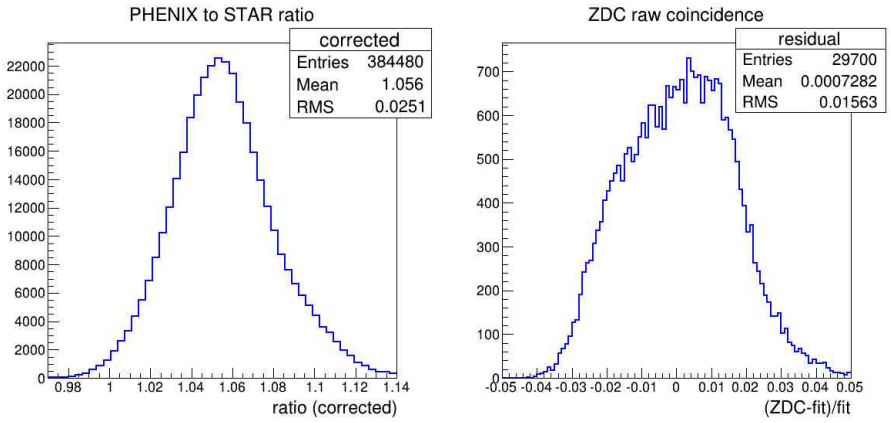

Figure 7: Left: deviation of the ratio PHENIX/STAR from a constant average for the week before store 18915. Right: ZDC raw signal residual from one randomly picked store shortly before store 18915.

itself changes as a function of time during the store and is applied point-by-point in 1 Hz intervals. In store 18915 it drops from about 40% at the beginning to about 15% at the end.

4.3 BPMs

Beam position measurements rely on the BPMs [7], here in particular the DX BPMs which are attached to the DX magnets, approximately 8 m from the the Interaction Point (IP). DX BPMs are in a common beam pipe and subjected to both beams. There are two components: relative and absolute accuracy. Relative measurements affect the measured step size in a vernier scan (see subsection 4.3.2). Absolute beam position measurement determine how well we can know the crossing angle (see subsection 4.3.1).

4.3.1 Beam Position at the IP and Crossing Angles

Unfortunately, in absolute terms the beam position measurement is difficult if not impossible to determine accurately. The position of the two beams at the IP, provided they are in optimized head-on collisions, should give the same value regardless of which beam is measured. The distance between the DX BPMs is 16.32 m at IP6. There is only a drift between the DX BPMs. DX BPMs have the extra difficulty - or advantage - that they are subject to both beams, hence any possible geometrical displacement in the device would apply to both beams and thus cancel out when the difference between the two beams is calculated. The position of the beam at the IP for one beam (blue or yellow) is given by

$$\mathrm{Pos_{IP}} = \frac{1}{2}\,(\mathrm{BPM_{in}} + \mathrm{BPM_{out}}), \tag{8}$$

with "in" and "out" referring to the two sides of the IP (in-coming and out-going). The difference Δ between the two beams according to the DX BPMs then follows:

$$\Delta_{\mathrm{DX}} = \mathrm{Pos_{IP}^{blue}} - \mathrm{Pos_{IP}^{yellow}}, \tag{9}$$

device	18676	18721	18776	18915_1	18915_2	18915_3	18943
$\Delta^{\mathrm{H}}_{\mathrm{DX}}$	235	260	306	261	264	253	247
$\Delta^{\mathrm{V}}_{\mathrm{DX}}$	-42	-17	2	10	8	1	17

Table 3: Measurements of the difference of the blue and yellow beam position at IP6 using DX BPMs from all 7 vernier scans in 2015. Units are μm.

where $\mathrm{Pos}_{\mathrm{IP}}$ is calculated according to Equation 8 above. This is done for the two planes and the two IPs separately. The results are summarized in Table 3 below.

The problem with these numbers is apparent. Taking the DX BPM measurements alone, the blue and yellow beams are separated by up to 300 μm or an average of 260 μm - while colliding head-on. Head-on collisions are guaranteed by the vernier scans and all data in Table 3 are taken right after a successful scan. In addition, the "fake" separation is not constant but varies from store to store by up to 70 μm Therefore the uncertainty in the determination of the absolute beam position at the IP when using the DX BPM is at least as large as the largest measured "fake" separation, i.e. 300 μm since we know that there was no separation of the two beams at the time. However, the measured false separation is consistent throughout the 100 GeV proton run in 2015.

Crossing angles can reduce the maximum collision rate to varying degrees depending on the bunch length and beam size. In order to determine this angle, all four DX BPMs in each plane on either side of the IP have to provide reliable and accurate absolute beam position measurements. The angle of one beam in mrad is calculated by the difference of the beam position on the in-coming and the out-going side divided by the distance between the two BPM (i.e. 16250 mm) and the total crossing angle between the two beams is given by:

$$\phi = \frac{(\mathrm{BPM}^{B}_{\mathrm{in}} - \mathrm{BPM}^{B}_{\mathrm{out}})}{16250} - \frac{(\mathrm{BPM}^{Y}_{\mathrm{in}} - \mathrm{BPM}^{Y}_{\mathrm{out}})}{16250}. \tag{10}$$

Fig. 8, left, shows the total crossing angles as measured by the DX BPMs in store 18915. It has an average value of 46 μrad in the vertical plane and is, averaged, negligible in the other. Keep in mind, that there is up to 0.016 mrad uncertainty due to inaccurate absolute position measurements. Combining the two, the larger measured angle and the

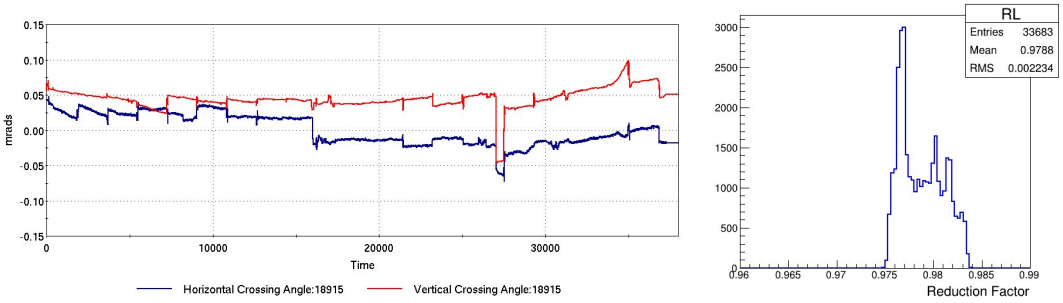

Figure 8: Left: Crossing angles as measured by the DX BPMs in store 18915. Right: Histogram of calculated Reduction Factors R_L, varying with the bunch length during store 18915.

larger uncertainty of the two planes, one can approximate the luminosity reduction factor

R_L due to a crossing angle:

$$R_L = \left[1 + (\frac{\sigma_z}{\sigma^*_{x,y}} tan\phi)^2\right] \tag{11}$$

where ϕ is half the crossing angle and $\sigma^*_{x,y}$ the horizontal or vertical beamsize at the IP, i.e. $\sigma^{VS}/\sqrt{2}$. R_L grows with the bunch length σ_z. Fig. 8, right, shows a histogram of the R_L values as it varies with the bunch length during store 18915. The mean reduction due to a potential worst-case crossing angle is 2%. The presence of a crossing angle will always reduce the rates and will never increase it. **Therefore, we will apply half of the maximum effect, i.e. 1%, as a correction and apply a symetric ± 1% systematic uncertainty to this effect**. This correction factor of 0.990 appears as R_{xang} in the equation for the fully corrected cross section, Eq. 12.

4.3.2 Step size

For Run-15, as well as for the PP2PP dedicated three vernier scans, the beam position "x" in both, Equations 1 and 2, is taken from the "set" value (i.e. from the model) when a vernier scan is performed. We have to establish how much of the "set" separation is actually executed to determine the accuracy of the measurement of the width of the overlap reagion. It appears, as indicated before and as can be seen in Fig. 2, bottom, when using the measured distances (by DX BPMs), the achieved χ^2/ndf are considerably larger than for the "set" values, which is why the latter were used to calculate the cross sections. In order to study the reliability of the distance measurement, DX BPM data is compared to the set value from the model for each plane and ring for every individual vernier scan from the 2015 pp100 run. Figure 9 shows one example. The data shown is taken during the vertical vernier scan 18915_3. The top left and right graphs show the variations of the blue beam as seen by the DXB5V (left) and DXB6V (right) devices while the yellow beam is moved across the blue. Since the yellow beam was moved, the visible motion of the blue beam is caused by the beam-beam effect [4]. The center left and right graphs show the movement of the yellow beam during the scan as seen by the sector 5 DX BPM (DxY5V) and the sector 6 DX BPM (DxY6V). In this particular case, DXY5V registers 9% more motion than asked for (i.e. 110 measured microns for every 100 set microns) while DxY6V registers 3% less. The combined effects, using Equation 8 to extrapolate to the IP, are shown in the bottom row.

Using all vernier scans, including the earlier scans from the pp100 run, a consistent and reproducible few percent motion more than were asked for were measured. Consistency and reproducibility in sign and amount indicate a systematic and non-statistical shift ("over-shoot") in the distance measurements when comparing the model with the DX BPM data and thus suggest reliability of the DX BPMs when used for relative measurements. The over-shoot applies to both planes and both rings in slightly varying amounts. There were 3 Blue and 4 Yellow scans in 2015:

BH mean: 1.063, stdv: 0.015

BV mean: 1.035, stdv: 0.008

YH mean: 1.066, stdv: 0.009

YV mean: 1.053, stdv: 0.006

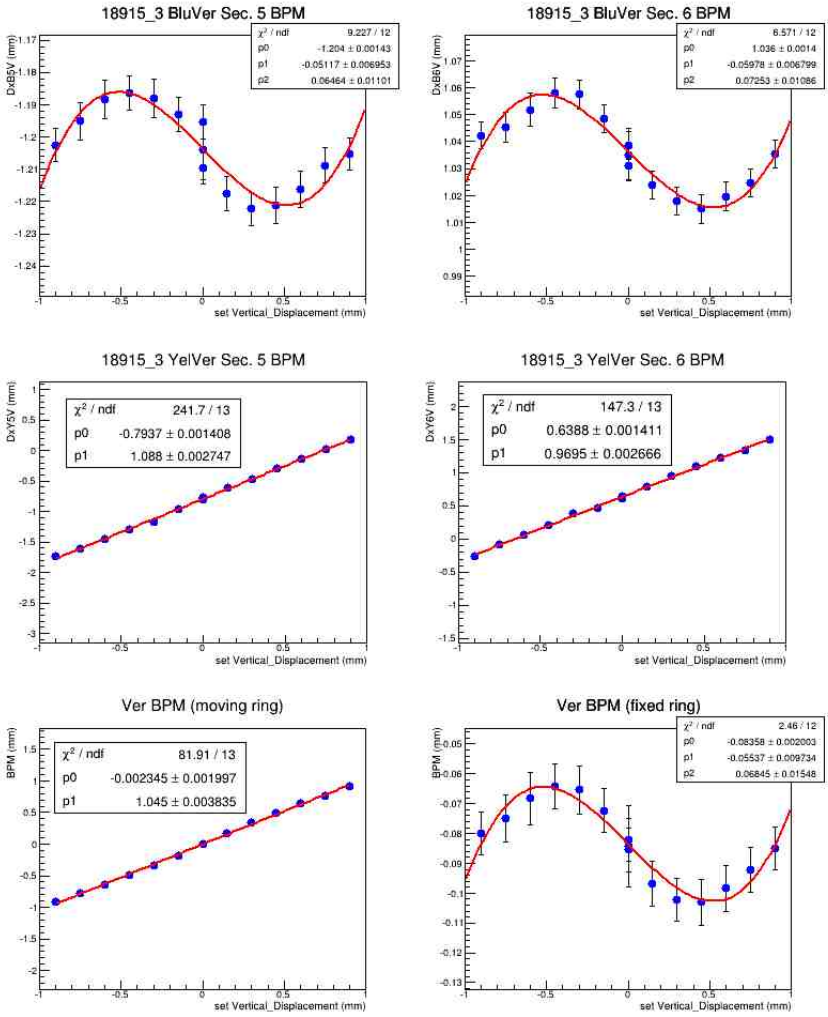

Figure 9: Measured beam positions as a function of set position (from model) during the vertical half of the vernier scan in IP6 during the scan 18915_3. The yellow beam was moved.

While the consistency of the over-shoot indicates a real effect, the also consistent bad χ^2/ndf values for the fits using the measured distances indicate large step to step fluctuations. Therefore, we will apply the mean values as a correction factor to the set values before fitting and calculating the cross sections. This correction does not appear in Eq. 12, the final fully corrected cross section because it is applied step by step when the data from the vernier scans is analyzed. This is necessary to provide for the individual corrections for the different rings and the two planes. This way, a correction factor of 1.035 can be applied to the vertical stepsizes during a blue scan while a correction factor of 1.066 is applied when analyzing a horizontal scan in the yellow ring. Using the standard deviations from above yields **a 3% systematic uncertainty in the cross section due to the lack of knowledge of the precise relation of model ("set" values) to real machine ("measured" values)**.

4.4 Hourglass Reduction

The hourglass reduction factor $R_{\rm hg}$ [8] represents a loss in luminosity due to geometrical effects for Gaussian beams. The geometrical effect is caused by the parabolic shape of the beta-function along z in the IP between the triplet quadrupoles. For this note, $R_{\rm hg}$ was calculated using the "StoreAnalysis" application [9]. Typically this factor ranges from about 0.6 to 0.75 for protons at 100 GeV in RHIC for the lattice that was used in 2015, depending on the bunch length (the longer the bunches, the smaller the reduction factor). In store 18915 it starts at about 0.77 and drops to 0.67. However, due to the distance of the ZDCs from the IP ($\approx$ 20 m), this geometrical effect has no implication on the effective cross section for this particular detector. At this distance the beam size simply appears enlarged by the hourglass effect leading to a collision rate that is reduced but the true rate none-the-less and no hourglass correction is needed for the ZDC detector. The measured effective cross section (see Eq. 3) is independent of the beta-function at the IP. The hourglass correction needs to be applied for effective cross section measurements of detectors that are closer to the IP center and emittance measurements. The hourglass enlarged beam width, as seen by the ZDC detectors, has to be projected to the 'true' width at the IP with a known value of β^* to calculate the emittance, if one would chose to do so.

5 Cross Section Results

The measured effective ZDC cross sections are summarized in Table 4 and shown in Fig. 10. Errors shown or listed are statistical only. Each individual cross section in Tab. 4 is

scan	σ_x [mm]	σ_y [mm]	$\sigma_{\rm eff}^{\rm ZDC}$ [mbarn]	$\mathcal{L}$ $[10^{31} cm^{-2} s^{-1}]$
	1G			
18915_1	0.309 ± 0.001	0.307 ± 0.001	0.293 ± 0.003	4.61 ± 0.05
18915_2	0.318 ± 0.001	0.322 ± 0.002	0.285 ± 0.003	4.05 ± 0.05
18915_3	0.329 ± 0.001	0.324 ± 0.001	0.284 ± 0.003	3.79 ± 0.04
	2G			
18915_1	0.312 ± 0.001	0.307 ± 0.001	0.301 ± 0.003	4.55 ± 0.05
18915_2	0.329 ± 0.001	0.327 ± 0.001	0.298 ± 0.003	3.90 ± 0.05
18915_3	0.336 ± 0.001	0.332 ± 0.001	0.301 ± 0.003	3.63 ± 0.04

Table 4: Fit parameters, effective cross sections and instantaneous luminosities for the two fitting approaches. Errors are statistical.

corrected for the effects listed above using the following:

$$\sigma_{\rm corrected}^{\rm ZDC} = \sigma_{\rm pre-corr}^{\rm ZDC} \times R_{debBeam} \times R_{FP} \times R_{xang}. \quad (12)$$

Note that $\sigma_{\rm pre-corr}^{\rm ZDC}$ is a cross section derived after some but not all corrections. It already contains a 1 Hz point-by-point correction for accidental coincidences (see section 4.2) as

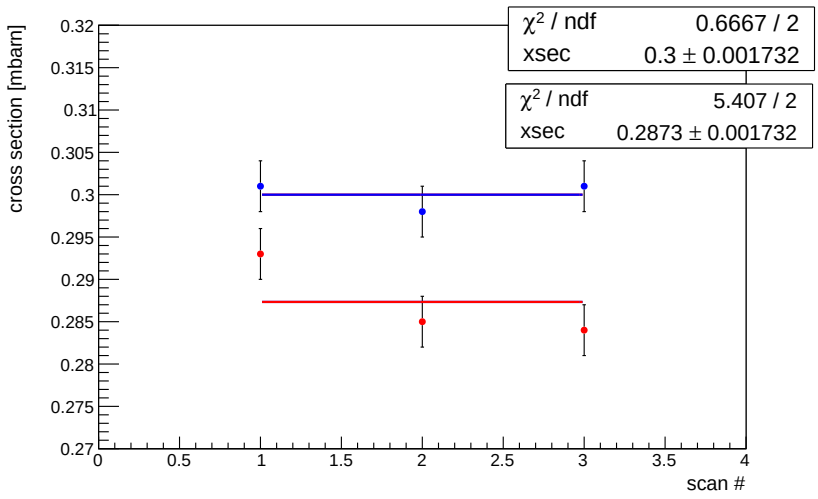

Figure 10: Cross sections using the 2G approach (blue points) and the 1G approach (red points).

well as a normalization of the beam intensity at each step of the vernier scan to compensate for a monotonously decreasing beam intensity while performing a scan. In addition, individual correction factors are applied to the set step-sizes, depending on plane and ring and varying from 1.035 to 1.066, see section 4.3.2 for details. And finally, details about $R_{debBeam}$ and R_{FP} can be found in section 4.1 and about R_{xang} in section 4.3.1 above. The final cross section combines the results from the two fitting approaches by averaging. Another 2% systematic error stemming from a lack of absolute knowledge of the beam shape is associated with it. To summarize, the systematic error contributions are as follows:

1. 0.2% DCCT accuracy
2. 1.0% bunched beam measurement (WCM and rebucketing)
3. 1.0% accidental coincidence correction
4. 3% width measurement (relative BPM, set vs measured)
5. 1% crossing angles (BPM, absolute)
6. 2% fit function, i.e. beam shape: 1G or 2G

Combining the corrections, statistical errors and the systematic errors (added in quadrature) from above, the resulting fully corrected effective cross section for the STAR PP2PP run in 2015 can be summarized to:

- $\sigma_{\text{eff}}^{\text{ZDC}} = 0.294 \pm 0.002$ (stat.) $\pm$ 0.012 (syst.) [mbarn]

References

[1] A. Baltz et al., Nucl. Instr. and Methods, A417 (1998) 1.

[2] S. Van Der Meer, ISR-PO/68-31, KEK68-64.

[3] Ted d'Ottavio, A. Drees, http://www.cadops.bnl.gov/Controls/doc/lisa/lisa.html

[4] K.A.Drees (BNL), S. White (CERN), "Vernier Scan Results from the First RHIC Proton Run at 250 GeV", IPAC10 Proceedings, 2010.

[5] http://www.cadops.bnl.gov/Instrumentation/InstWiki/index.php/RHIC_Current_Transformer

[6] D. Cronin-Hennessy, A. Beretvas and P.F. Derwent, "Luminosity monitoring and measurement at CDF", Nucl. Instruments and Methods A433 (2000) 37

[7] R. Michnoff et al., "RHIC BPM SYSTEM AVERAGE ORBIT CALCULATIONS", PAC proceedings, 2009.

[8] M.A. Furman, "Hourglass Effects for Asymmetric Colliders", PAC Proceedings, 1991.

[9] StoreAnalysis application, S. Binello, W. Fischer, private communication

[10] R. Connolly et al., "RESIDUAL-GAS-IONIZATION BEAM PROFILE MONITORS IN RHIC", Proceedings of BIW10 Conference, Santa Fe, New Mexico, US, 2010.